



Evaluation of pre-ionized argon test flow conditions in the T4 reflected-shock tunnel for hypersonic air-breathing electromagnetic propulsion experiments

A. Lefevre, A. Garnier, V. Wheatley, T.J. McGuire, A. Paull, N. Temme⁶

Abstract

The use of argon test gas in the T4 Stalker tunnel is numerically investigated by means of the L1D and NENZF1D facility simulation codes, with the aim of producing pre-ionized argon experiments for future fundamental studies of hypersonic, airbreathing electromagnetic propulsion. The results computed with Mach 4 and Mach 7 nozzles indicate that significant non-thermal ionization fractions ranging from 1.0e-6 to 3.0e-3 can be produced in the experimental test flow, with corresponding electrical conductivities of up to 100 S/m. A quasi-1D, steady-state solution was then applied to evaluate MHD source terms and solve the Navier-Stokes equations with a simple first-order Euler scheme. Joule heating was found to be significant when constant electric field acceleration was attempted, preventing any significant acceleration of the flow, which nonetheless provides a good case for fundamental studies of Joule heating effects on flow structure in non-equilibrium, weakly ionized plasma. Options for improving the Lorentz efficiency and thrust performance are proposed for future studies. Experimental characterization of these new argon conditions should be performed, as well as more realistic CFD in three-dimensions, to go beyond the simplifying assumptions made in this preliminary study.

Keywords: hypersonics, magnetohydrodynamics, plasma, propulsion

Nomenclature

Latin	p – pressure, Pa
	T – temperature, K
A – area, m^2	u – velocity, m.s $^{-1}$
${f B}$ - magnetic flux density vector, T C_T - thrust coefficient	Greek
d_T – diaphragm thickness, mm	α – degree of ionization
e - electron elementary charge (1 C)	β – hall parameter
E – electric field vector, V m ⁻¹	ϵ – specific internal energy, J kg $^{-1}$
F – thrust, N	ϵ_0 – electric permittivity of free space, F m $^{-1}$
H – enthalpy, J kg $^{-1}$	η_L – Lorentz efficiency
\mathbf{j} - current density vector, A m $^{-2}$	γ – specific heat ratio
$k_b = 1.38e - 23$ – Boltzmann constant, J K ⁻¹	μ_0 – magnetic permeability of a vacuum, H m $^{-1}$
m_e – mass of an electron, kg	$ u$ – collision frequency, s $^{-1}$
n – number density m $^{-3}$	$ ho$ — density, kg m $^{-3}$

¹Centre for Hypersonics, School of Mechanical and Mining Engineering, University of Queensland, St Lucia, Australia, a.lefevre@uq.edu.au

HiSST-2025-141 Page | 1

²ISAE-ENSMA, Chasseneuil-du-Poitou, France, antoine.garnier@etu.isae-ensma.fr

³Centre for Hypersonics, School of Mechanical and Mining Engineering, University of Queensland, St Lucia, Australia, v.wheatley@uq.edu.au

⁴Lockheed Martin Corporation, tom.mcguire@Imco.com

⁵Centre for Hypersonics, School of Mechanical and Mining Engineering, University of Queensland, St Lucia, Australia, a.paull@uq.edu.au

⁶Centre for Hypersonics, School of Mechanical and Mining Engineering, University of Queensland, St Lucia, Australia, n.temme@uq.edu.au

 σ – scalar electrical conductivity, S m $^{-1}$ en - electron-neutral ω – gyrofrequency, s⁻¹ i - ion Subscripts in - engine inlet x,y,z - vector components in cartesian coordi- ST - shock tube t - translational or total e - electron/electronic or exit * - sonic condition

1. Introduction

Current propulsion technologies for air-breathing hypersonic flight, such as scramjets, have physical limitations inherent to the kinetics of the burning propellant, as well as the pressure requirements inside their combustion chamber. These mean that a scramjet becomes less efficient as altitude and Mach number increase and basically becomes inoperable at altitudes above 50 km, and no more efficient than rocket propulsion when flying above Mach 10-12. In contrast, Air-Breathing Electromagnetic Propulsion (EP) (illustrated in Fig. 1) does not require any propellant to be carried on board, and instead uses magnetohydrodynamic (MHD) effects to generate thrust directly from the engine inflow. The air passing through the engine only requires a small fraction of charged particles in order to produce usable thrust levels for hypersonic flight, and these particles can be produced from an energy-efficient source such as an electron-beam [1]. Electromagnetic Propulsion does not require any specific pressure for burning propellants inside the engine, which theoretically allows it to function efficiently at any atmospheric altitude up to Low Earth Orbit (LEO). Instead, the performance of an EP engine depends essentially on its ability to store and deliver electric power to electrodes and magnets producing the electromagnetic fields, and to the ionization source.

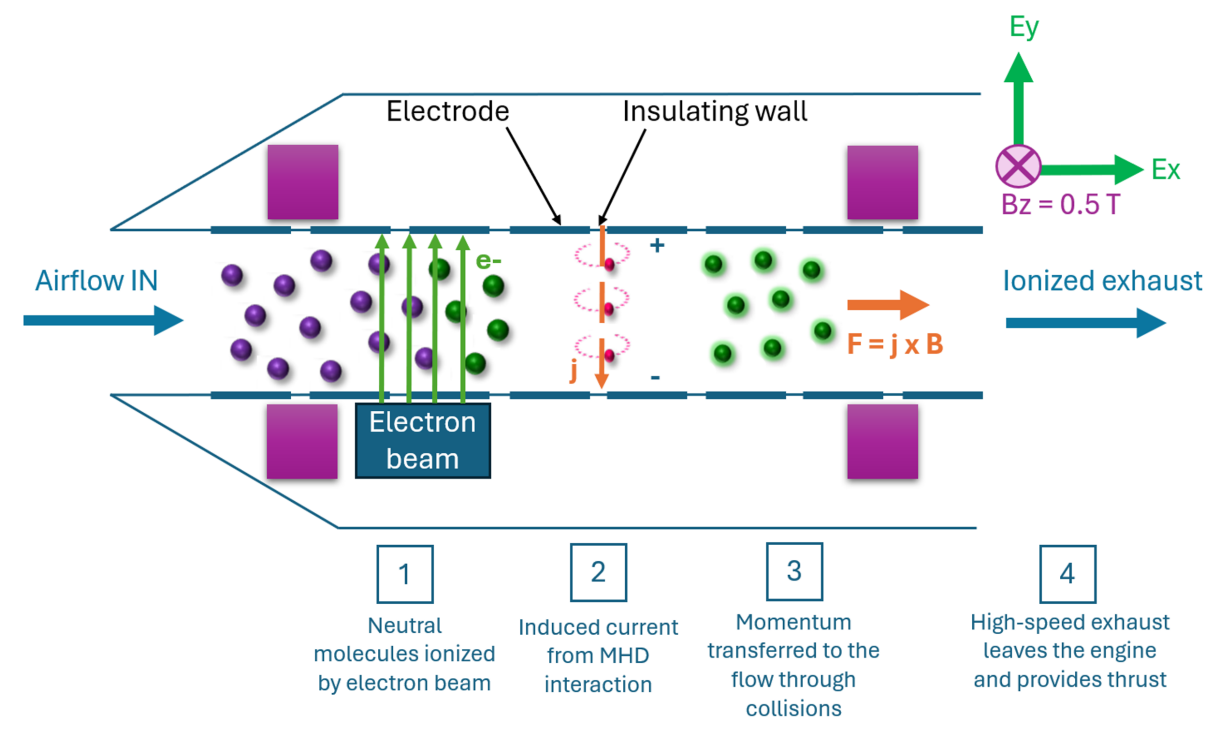


Fig 1. Conceptual diagram of an electromagnetic propulsion engine using an electron beam to generate thrust.

To date, hypersonic air-breathing electromagnetic propulsion remains mostly unexplored, with no ground or flight-testing data available. A few numerical studies have shown promising results, however [1, 2]. Before a practical EP Engine can be produced, several unknowns must be addressed that are specific to hypersonic air-breathing flight. Indeed, the impact of phenomenon such as Hall effects, Joule heating, plasma sheaths, and electron recombination on the engine performance remains unknown.

The T4 reflected shock tunnel at the University of Queensland [3, 4] has the ability to generate hypersonic air flows ranging from Mach 4 to Mach 12, while producing flight-realistic electrodynamic boundary conditions, which are characterized by a cold, non-ionized freestream with pressure and velocity matching what would be encountered in flight at altitudes ranging from 20 to 50 km. Such experimental conditions would be suitable for investigating an electron-beam powered EP engine. On the other hand, in order to better understand the fundamental physics parameters that drive these engines, a more decoupled approach would be beneficial. In particular, if a set of pre-ionized test flow conditions could be produced, the complex physics and interactions of the electron beam with the plasma flow could be removed (as in Section III.B of Ref [2]). While the T4 shock tunnel does not produce any usable pre-ionization when operated with an air test-gas, an argon test-gas could in theory become strongly ionized in the stagnated region at the end of the shock tube section (also called nozzle supply). The subsequent nozzle expansion of this stagnated gas can then partly freeze the electron recombination processes so that a usable degree of ionization remains in the nozzle exit test flow. This has the added advantage that the nozzle exit flow temperature may remain cold, with no significant equilibrium ionization, thus maintaining realistic electrodynamic boundary conditions and avoiding potential MHD instability issues described in Ref [1]. If verified, such flow conditions could prove particularly suitable for fundamental studies of electromagnetic propulsion physics. Argon has never been used as a test gas in T4, however, and potential experimental conditions have not yet been evaluated.

The aim of this paper is to numerically predict the argon test gas properties (and especially the ionization fraction) that can be expected within the T4 operating envelope, and to evaluate the suitability of such flow conditions for future electromagnetic propulsion experiments.

2. Numerical implementation

2.1. Governing equations

A viscous flow interacting with a magnetic field is governed by Navier-Stokes equations for the fluid dynamic aspect, with the equations of mass, momentum and energy conservation in differential form (Eq. (1) to Eq. (3)); and Maxwell's equations (Eq. (4) to Eq. (7)) for the electrodynamic aspect, which describe electromagnetic fields and how they evolve in time:

$$\frac{\partial \rho}{\partial t} + \nabla \cdot (\rho \mathbf{u}) = 0 \tag{1}$$

$$\frac{\partial \rho \mathbf{u}}{\partial t} + \nabla \cdot (\rho \mathbf{u} \mathbf{u} + p \mathbf{I} + \tau) = \mathbf{j} \times \mathbf{B}$$
 (2)

$$\frac{\partial \rho E}{\partial t} + \nabla \cdot ((\rho E + p + \tau)\mathbf{u} + \mathbf{q}) = \mathbf{j} \cdot \mathbf{E}$$
 (3)

$$abla \cdot \mathbf{E} = rac{
ho_e}{\epsilon_0}$$
 (4)

$$\nabla \cdot \mathbf{B} = 0 \tag{5}$$

$$\nabla \times \mathbf{E} = -\frac{\partial \mathbf{B}}{\partial t} \tag{6}$$

$$\nabla \times \mathbf{B} = \mu_0 \mathbf{j} + \epsilon_0 \mu_0 \frac{\partial \mathbf{E}}{\partial t}$$
 (7)

To complete this set of equations, the current density \mathbf{j} (provided by the generalized Ohm's law [5]) and charge conservation are respectively expressed as follows:

$$\mathbf{j} = \sigma(\mathbf{E} + \mathbf{u} \times \mathbf{B}) - \frac{\beta}{\mathbf{B}}(\mathbf{j} \times \mathbf{B}) + (1 - \alpha^2) \frac{\beta_e \beta_i}{B^2} [(\mathbf{j} \times \mathbf{B}) \times \mathbf{B}]$$
(8)

$$\frac{\partial \rho_e}{\partial t} + \nabla \cdot \mathbf{j} = 0 \tag{9}$$

2.2. Quasi-1D solution for a rectangular engine

2.2.1. Engine geometry

The proposed geometry shown in Fig. 2 is being considered for future experiments of electromagnetic propulsion at the University of Queensland (UQ). It has a long enough channel for significant acceleration to occur (in the right conditions), and its cross-sectional area would allow it to fit inside test sections of T4 as well as other facilities available at UQ (such as expansion tubes for higher velocity tests). Furthermore, for the proposed 20 mm cross-section, a fairly uniform magnetic flux density of 0.5T can be easily achieved with permanent neodymium magnets (N52 class) placed on either side of the channel (facing the z-axis in Fig. 2). Multiple pairs of electrodes would then be placed along the channel and facing each other along the y-axis.

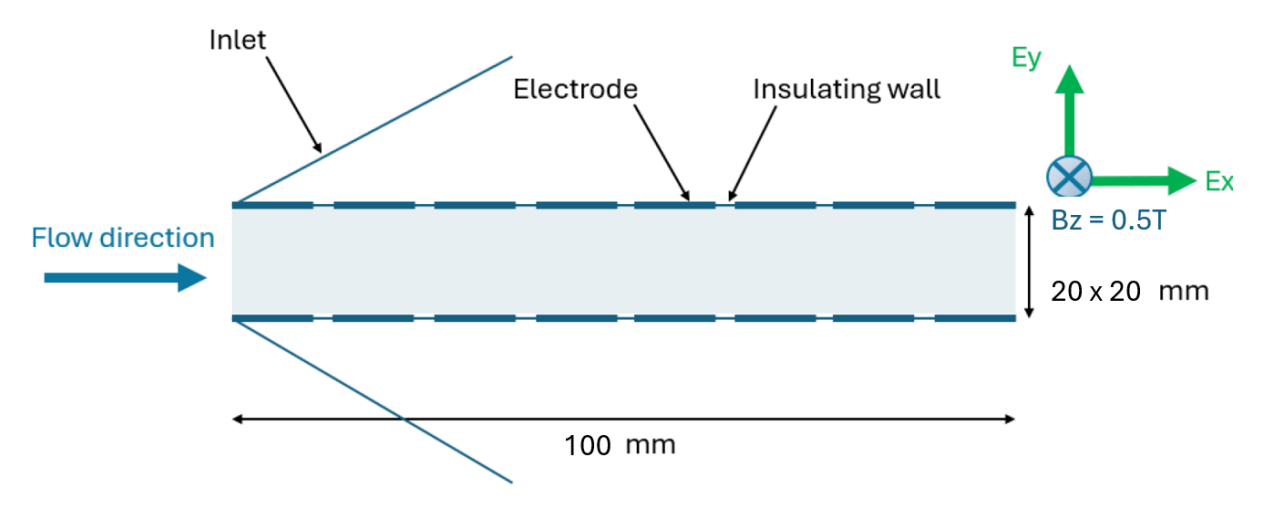


Fig 2. EP engine geometry

2.2.2. Approach

Although realistic 2D/3D simulations are necessary to model the complex MHD physics at play in an EP engine, they are typically computationally expensive. For the purpose of a preliminary study where the aim is to map electromagnetic propulsion performance across a wide range of potential experimental conditions, a simpler solution may be used, as long the right simplifying assumptions can be made. The validity of these is part of the study's discussion adn will form the basis of future, more refined studies. In this section, a quasi-1D solution is formulated based on the following:

- A uniform, static magnetic field is applied along the z-axis. Induced magnetic fields are neglected (low magnetic Reynolds number assumption).
- A constant, transverse (y-axis) electric field is applied along the entire length of the accelerator channel.
- Hall effects are compensated by applying an axial E field component $E_x = \beta(E_y uB_z)$ to cancel any asymmetric terms in EQ. 8. This leads to the assumption that the induced current ${\bf j}$ is uni-directionnal in the y-axis, and that the Lorentz force has only an x-component (no transverse force). So while the electric field is effectively two-dimensional, this allows to solve a quasi-1D MHD problem.
- The electric field is prescribed directly by the applied potential difference across each electrode pair. Electrode sheaths and plasma potential effects on the electric field distribution are

assumed negligible.

- Argon flow: The engine flow is assumed to be inviscid, chemically frozen (no changes to the
 chemical species fractions), and at steady-state. It is also assumed that the argon inflow is
 undisturbed by the inlet geometry (no normal or oblique shocks at the inlet), which is reasonable
 as long as the leading edges are sharp.
- A 1st-order Euler scheme is implemented to solve a 1D, steady-state formulation of the Navier-Stokes and MHD equations.

2.2.3. MHD source terms

Electrical conductivity

In addition to the applied magnetic and electric fields, the magnitude of the interaction between the fields and the plasma flow is driven by the electrical conductivity. In this context the expected plasma is weakly ionized, and a conductivity model from Raizer [6] was used, that applies specifically to weakly ionized argon:

$$\sigma = 2.82 \times 10^{-4} \frac{n_e}{\nu_m} \tag{10}$$

where for argon, Ref [6] gives $\nu_m/p = 5.3 \times 10^9 s^{-1}.Torr^{-1}$.

Hall parameter

The electron Hall parameter is the ratio of their gyro-frequency under the magnetic field to the total collision frequency, and can also be defined as a function of the electrical conductivity:

$$\beta = \frac{\sigma B}{n_e e} \tag{11}$$

In this context the ions have a negligible Hall parameter, so it is assumed that $\beta \approx \beta_e$. This also means that the ion slip parameter $(\beta_e\beta_i)$ is usually small or negligible for most air-breathing EP applications. Furthermore, as stated in Section 2.2.2, the asymmetric terms can be cancelled by applying $E_x = \beta(E_y - u_x B_z)$. In this context the induced current density then simply becomes: $j_y = \sigma(E_y - u_x B_z)$.

Joule heating

Collisions between conducting charged particles and neutrals add energy into the flow, referred to as Joule heating, with the corresponding source term to the energy conservation equation:

$$\mathbf{j.E} = u_x j_y B_z + \frac{j_y^2}{\sigma} \tag{12}$$

2.2.4. Performance metrics

For a constant area duct, the thrust can be written as:

$$F = A_{duct}(\rho_e u_e^2 - \rho_{in} u_{in}^2 + p_e - p_{in})$$
(13)

and the thrust coefficient is defined as:

$$C_T = \frac{2 \times F}{\rho_0 u_0^2 A_{duct}} \tag{14}$$

The Lorentz efficiency is defined as the ratio of the energy source that goes into the plasma acceleration by the energy goes into heating the flow [2]:

$$\eta_L = \frac{\int ujBdx}{\int jEdx} \tag{15}$$

2.3. The T4 Stalker tunnel

The operating concept of the T4 reflected shock tunnel, or Stalker tunnel, is illustrated in Fig. 3. A free-driven piston is held in place by a vacuum cavity while high pressure air is filled behind it (Reservoir section). When the cavity is leaked to atmospheric pressure, the piston launches itself with considerable kinetic energy into the driver tube, inside which a helium/argon mixture is compressed until the metallic diaphragm isolating the driver tube and shock tube ruptures. When this happens a primary shock wave processes the test gas (argon in this study, but usually air), imparting energy to it in the form of velocity, temperature and pressure. When the primary shock wave hits the end of the shock tube, it bursts a thin mylar diaphragm of much smaller area, and reflects back towards the driver tube. The operating conditions are such that this reflected wave effectively stagnates the test gas to stagnation pressures ranging from 10 to 90 MPa, and enthalpies ranging from about 5 to 30 MJ/kg. The small mylar diaphragm is the start of a de Laval nozzle expansion with converging subsonic section, a throat where the gas passes Mach 1, and a diverging supersonic section, at the end of which the test gas exits the nozzle into the test section, with the desired hypersonic flow properties.

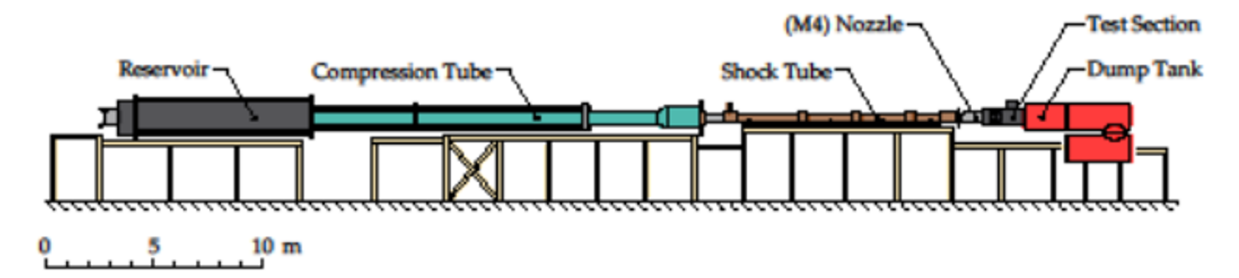


Fig 3. Conceptual diagram of the T4 Stalker tunnel

2.4. Numerical simulations of T4 flow conditions

L1D [7, 8] is a quasi-1D gas dynamics code that is applied to the simulation of entire shock-tube or expansion tube facilities. It has the ability to simulate the piston dynamics and shock wave processes occuring in the driver and compression tubes of T4, which allows to get an estimate of the stagnated test gas properties prior to its expansion in the nozzle. Once the nozzle supply conditions are known from L1D, the nozzle expansion that generates the experimental test flow in the T4 test section is calculated using NENZF1D [9], which is a program for estimating flow conditions in reflected-shock tunnels, when the test gas reaches temperatures high enough for chemical reactions to occur and when nonequilibrium chemistry effects are expected to be important. The calculation proceeds in two parts. Assuming thermochemical-equilibrium, a state-to-state calculation is done for the initial (subsonic) expansion of the test gas until it reaches sonic conditions at the nozzle throat. Then a calculation with finite-rate chemical reactions is made of the supersonic flow of the gas through the nozzle expansion. The finite-rate chemistry is particularly important for estimating the argon degree of ionization at the nozzle exit. Most of the operating parameters and nozzle designs used with NENZF1D can be found in Chan et al. [10].

3. Results

3.1. T4 nozzle supply

The L1d code was ran for 120 operating parameters of the T4 tunnel. 6 primary diaphragm thicknesses were considered (from 1mm to 6mm), and 20 initial shock tube fill pressure values (p_{ST}) ranging from 5 kPa to 500 kPa. The driver gas composition was fixed at 80% He - 20% Ar. Example traces of stagnation pressure at the nozzle supply are shown in Fig. 4, and the corresponding Ar+ mass fractions are shown in Fig. 5.

Stagnation pressure traces in Fig. 4 can indicate how well taylored the conditions are. In this example, the relatively flat supply pressure following the sudden initial rise (from the reflected shock wave processing) lasting for about 1-2 ms indicates a tailored condition for shock tube pressures ranging from 5 kPa to about 45 kPa. These usually produce fairly steady experimental test flows (for 2-3 ms), although p_{ST} values below 20 kPa have typically produced very small or inexistant experimental test times (0-0.1

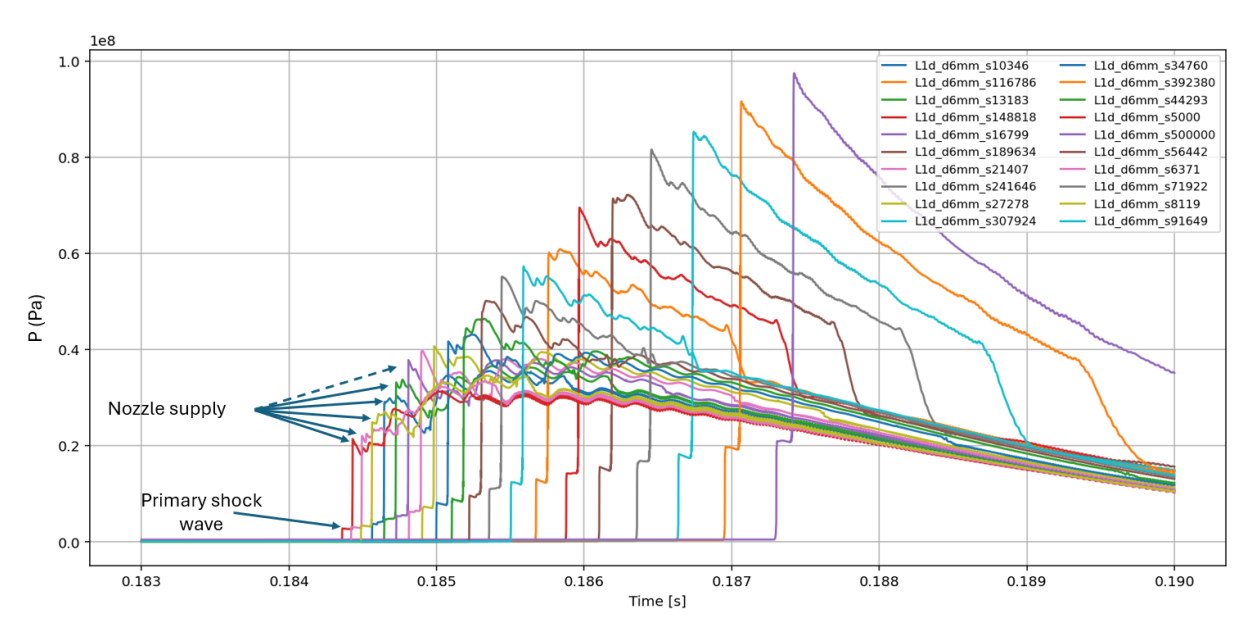


Fig 4. L1d pressure traces for varying shock tube argon fill pressures, using a 6 mm thick diaphragm

ms), due to the lack of available mass of test gas. Pressure traces for $p_{ST} > 45$ kPa show increasing negative gradients after the initial peak which indicates over-tailoring of the conditions. These typically produce less steady flow conditions with reduced test times. The piston/driver compression dynamics could be better tuned to improve the condition quality in future studies. However, in the context of this preliminary study, these conditions are still useful to evaluate the magnitude of argon ionization in the test flow. Importantly for the prospect of electromagnetic propulsion experiments, Fig. 5 shows very significant amounts of ionized Ar+ in the nozzle supply gas, as high as 61% for the 6mm diaphragm/ 5 kPa shock tube case.

3.2. Experimental test flow

The nozzle supply results provided by L1D were used as a starting point for finite-rate nozze expansion calculations using the NENZF1D code. For this study, two nozzles were considered which are commonly used with the T4 facility: the M4B and the M7B nozzles [10]. The M4-M7 denomination refers to the exit Mach number that the nozzles were designed to produce for an air test gas. M4B is 0.51m long and features an area ratio of 14.6, while M7B is 1 meter long with an area ratio of 169.2. For an ideal gas, the exit-to-throat area ratio is related to that of the Mach number by the following isentropic relation:

$$\frac{A}{A^*} = \frac{1}{M} \left[\frac{2}{\gamma + 1} \left(1 + \frac{\gamma - 1}{2} M^2 \right) \right]^{\frac{\gamma + 1}{2(\gamma - 1)}},\tag{16}$$

where for ideal air, $\gamma_{air}=1.4$, while for ideal argon $\gamma_{Ar}=1.667$. Subsequently, the expected exit Mach number for an ideal argon gas is 5.88 for the T4 M4B nozzle, and 13.9 for the T4 M7B nozzle. A two-temperature argon gas model based on Hoffert [11] was used in combination with a three-species reaction scheme. The properties of the nozzle exit test flow are plotted in Fig. 7 for the M4B nozzle, and in Fig. 6 for the M7B nozzle.

The first observation from Fig. 6 and Fig. 7 is that significant ionization degrees ($>10^{-6}$) can be expected for a large portion of the P_{ST} - d_T operating envelope of the T4 facility.

In terms of sensitivity to the diaphragm thickness and to the initial shock tube fill pressures, the exit test flow velocity, pressure, temperature and ionization degree are highest for the areas of lowest shock tube pressure and highest diaphragm thickness, and so is the flow enthalpy. Indeed, the thicker the diaphragm is, the higher its burst pressure is as well as the energy transferred to the compressed driver

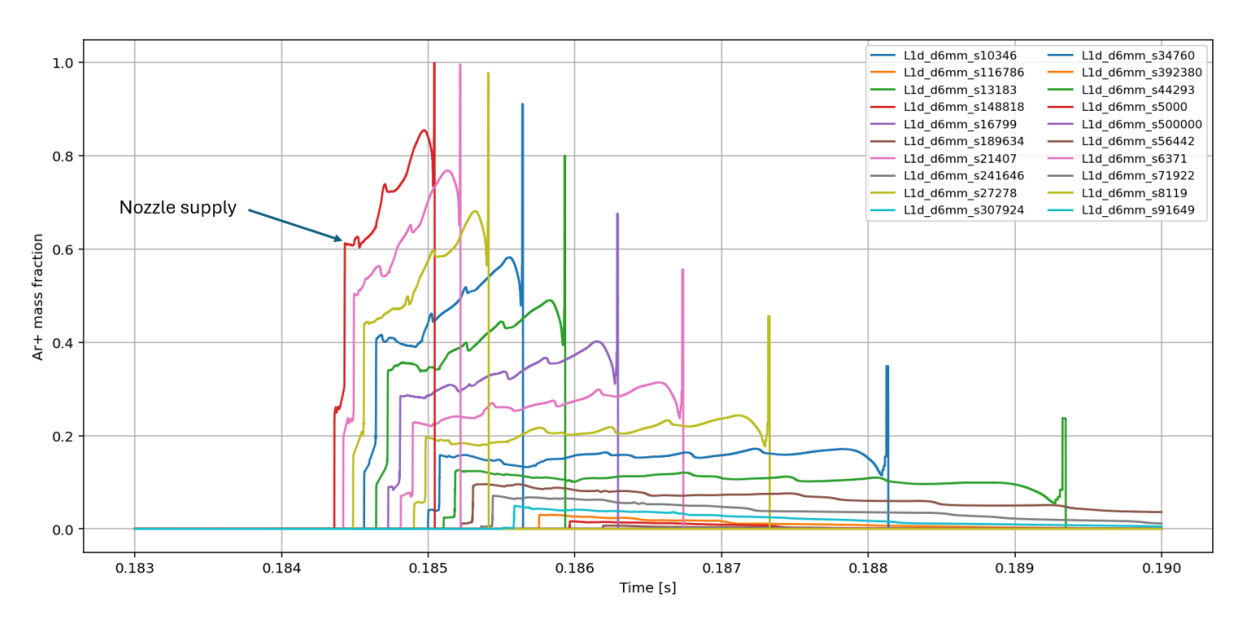


Fig 5. L1d - mass fractions of ionized argon at the nozzle entrance for varying shock tube argon fill pressures, using a 6 mm thick diaphragm

gas. This explains why flow enthalpy, temperature and pressure increase along with the diaphragm thickness. Additionally, the velocity of the primary shock wave in the shock tube increases as the intial fill pressure decreases, which leads to more compression and energy transfer to the argon test gas, and therefore to higher flow enthalpies. Meanwhile, the degree of ionization at the nozzle seem to mostly align itself with the variations of flow enthalpy. Higher enthalpies indeed translate into increased nozzle supply temperatures and equilibrium ionization of the test gas, and for the same nozzle the remaining ionization at the exit mainly depends on that initial supply ionization.

An interesting phenomenon is how the nozzle exit Mach number is not uniformly distributed over the T4 operating envelope. Instead, the value converges to the ideal gas prediction of 13.9 for the M7B nozzle, and of 5.88 for the M4B nozzle, and this occurs at the higher shock tube fill pressures. Meanwhile, at the lowest bound of P_{ST} , the Mach number varies from 7.2 (6mm diaphragm) to 13.5 (1mm diaphragm), and this gap reduces as P_{ST} increases. The most likely explanation is that the effective γ_{Ar} is reduced at flow conditions where there is a significant fraction of energy going into electronic excitation and ionization kinetics of the Argon molecules, which occurs with the lower P_{ST} / higher d_T inputs. With more energy stored into each single argon molecule, the heat capacities ($C_{p_{Ar}}$ and $C_{v_{Ar}}$) increase, which has the effect of reducing γ_{Ar} . And per EQ. 16, the exit Mach number is proportionally reduced. As flow temperature and ionization fraction drops when P_{ST} reaches the top of the envelope, the test gas becomes more "ideal" and the resulting exit Mach number reaches the expected values.

The choice of driver gas composition for this study was narrowed to only one combination which was mostly arbitrary. For future experimental designs, this can be tuned to achieve more specific test flow conditions. Driver mixtures with more argon content tend to produce lower shock speeds and enthalpies, with correspondingly lower test gas velocities, while increasing the Helium fraction allows for a higher test gas velocity envelope. This is because helium has a much higher sound speed than argon, producing higher velocity shock waves that transfer more energy to the test gas.

With regards to temperature, it is important to note that the two-temperature model is only designed to give a valid calculation of the electronic temperature as long as T > 3000K, which is an important consideration for the kinetics involving reactions with electrons which are controlled by the electronic temperature. The implementation of the model in UQ's CFD code added safeguards so that reactions become frozen if the temperature goes below the validity threshold of 3000 K. This is not expected to

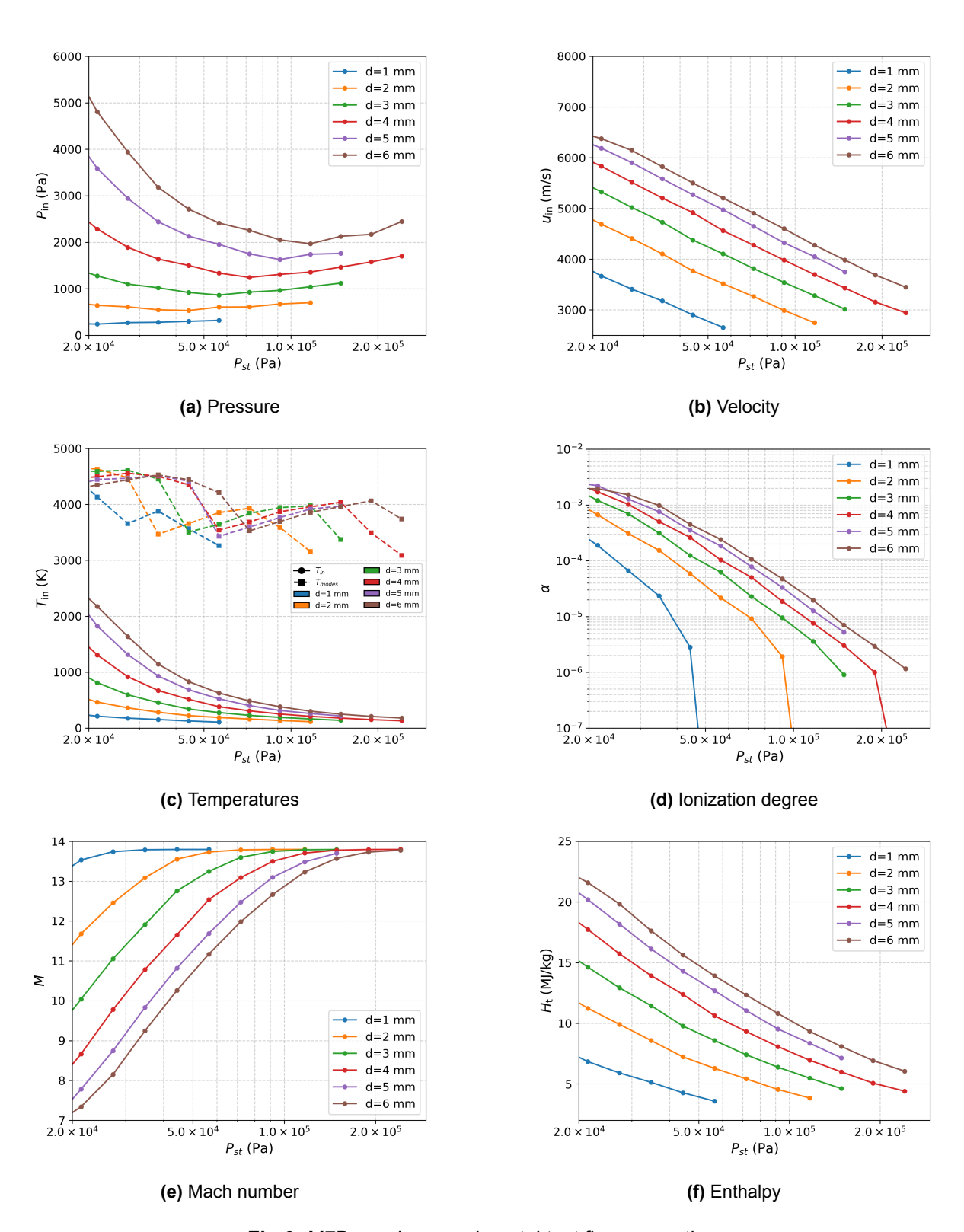


Fig 6. M7B nozzle, experimental test flow properties

significantly affect the exit flow composition, since the chemistry is already mostly frozen before the

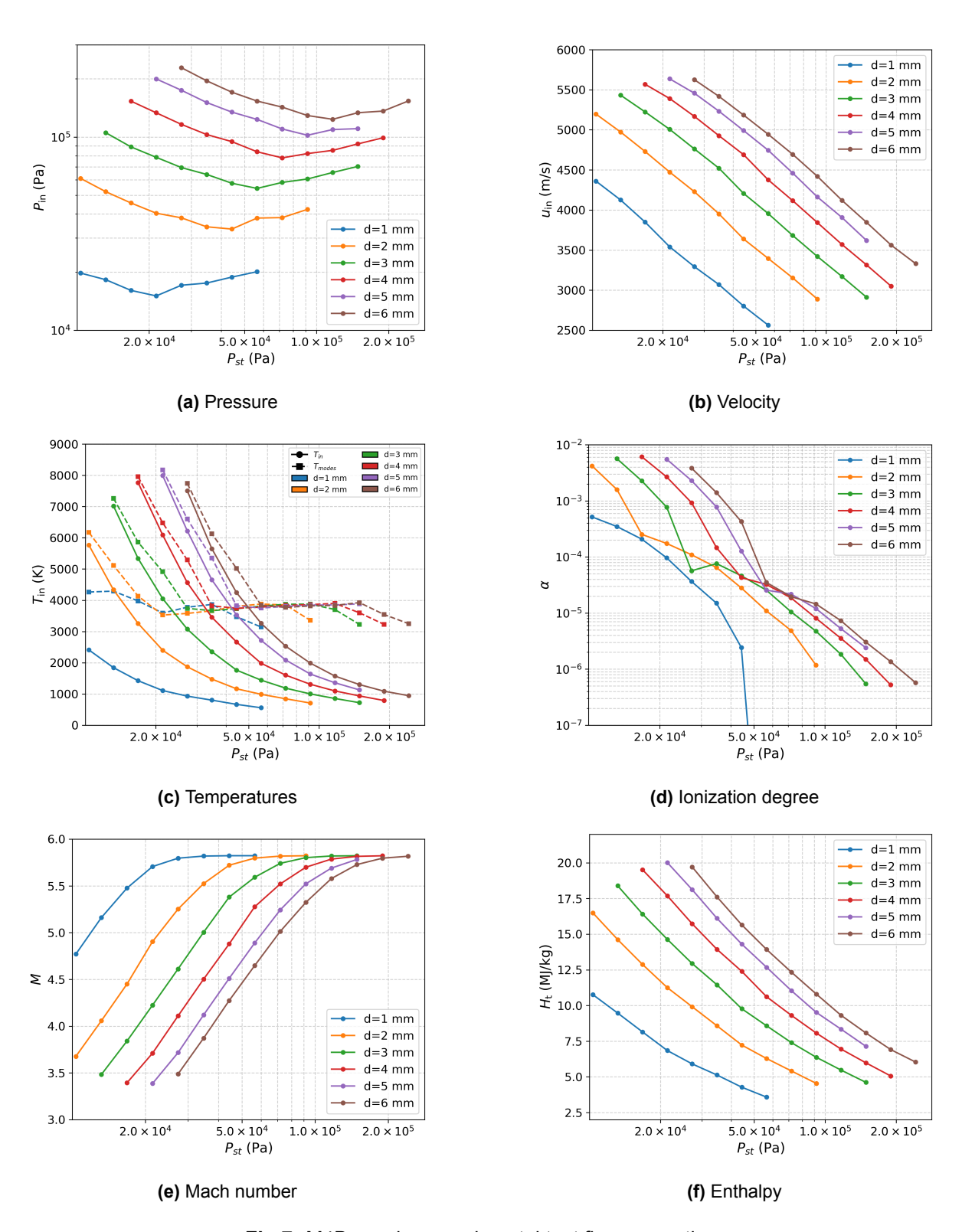


Fig 7. M4B nozzle, experimental test flow properties

temperature threshold is breached. This also means that the electronic temperature of the exit flow is

not exactly known in these cases, and the results shown in Fig. 7-6 show the last known T_e values, at the exception of the few M4 conditions where temperature of the exit flow remained high enough for the argon model to keep solving T_e . In future studies, the model should be refined so that the validity range can be extended to colder, low density argon flows.

Other nozzles are available for T4 operation, featuring various area ratios (for M6, M8 and M10 air gas), however their study was out of scope for the current paper. For conciseness, the electromagnetic propulsion results of the next section will focus on the M7B nozzle conditions, which produced test flows more characteristic of what will likely be encountered in actual hypersonic flight.

With the available choice of diaphragm thicknesses and shock tube pressures, it is possible to select conditions featuring a wide range of ionization fractions, while maintaining other flow properties fairly constant (iso-velocity, pressure, Hall parameter etc.), and vice-versa. Table 1 shows examples of isovelocity test flow conditions for the M7B nozzle, where the ionization fraction varies by about two orders of magnitude, while the flow velocity and temperature are mostly constant. A maximum applicable electric field is listed in Table 1, based on Paschen's law [12], which informs on the maximum applicable electrode potential difference before an arc would occur.

$\overline{d_T}$	$p_{ST}\left(kPa ight)$	$u_{in}\left(m/s ight)$	α	$T_{in}\left(K\right)$	$p_{in}\left(kPa\right)$	$\sigma\left(S/m\right)$	$\boldsymbol{\beta}$	$E_{Paschen}\left(V/m ight)$
3 mm	27	5000	7.0e-4	590	1.1	34	0.5	37970
4 mm	40	5000	3.5e-4	560	1.5	13	0.6	48009
5 mm	55	5000	1.9e-4	530	2.0	11	0.7	58783
6 mm	68	5000	1.2e-4	510	2.3	10	0.8	65752

Table 1. Examples of constant velocity conditions with varying ionization fractions; for M7B nozzle

Note that, typically, accurate predictions of experimental test flow properties in L1D and NENZF1D are possible thanks to empirical tuning of some of the input parameters (flow losses, boundary layer effects in nozzle, etc.), based on experimental characterizations using Pitot pressure measurement data. Since no such characterization has been performed yet with argon test gas, the conditions proposed in Table 1 are only preliminary estimates, and more refinement will be required before a final set of conditions can be selected for future experiments.

3.3. Electromagnetic propulsion

3.3.1. MHD parameters

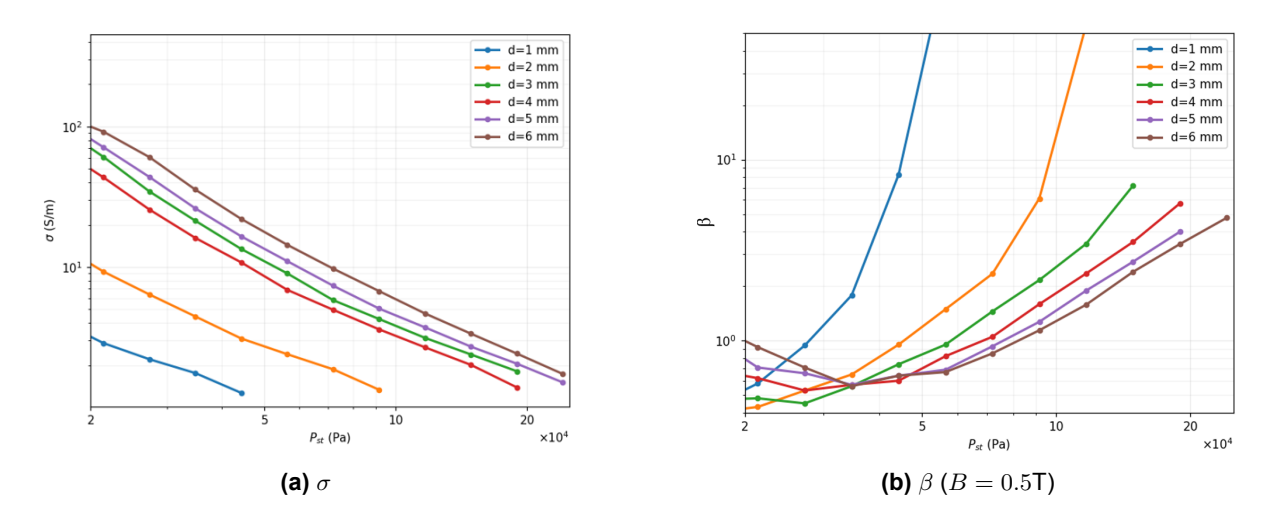


Fig 8. Electrical conductivity and Hall parameter for the M7B conditions

It is useful to characterize the plasma generated by the T4-produced argon conditions in terms of electrical conductivity and Hall parameter. As shown in Fig. 8, electrical conductivity values of up to 100 S/m are available within the flow conditions envelope. Assuming $B_z=0.5$ T, the corresponding Hall parameter ranges from 0.1 to 8.0. For pure "Faraday" mode acceleration (mostly transverse E field), the Hall parameter should be smaller than 1.0. This is the case here for most conditions where the electrical conductivity is also high. For conditions where β is greater than 1, an electromagnetic propulsion engine would have to operate in "Hall" mode instead, where the electric field is predominantly axial in order to produce transverse induced currents and axial Lorentz force only (for thrust production). In real flight, Hall mode acceleration would usually become necessary in the low density, upper altitudes of the Earth atmosphere, where low collision rates allow high-levels of electron mobility and magnetization. In this study, conditions of interest for EP experiments would likely target the low p_{ST} values where the electrical conductivity is the highest and where the Hall parameter is small.

3.3.2. Performance metrics - E = 7.5 kV/m

In this section some important performance metrics are plotted across all the available M7B conditions, starting with a moderate electric field strength of 7.5 kV/m. This was found to be sufficient to illustrate the key mechanisms driving the performance at these particular test conditions. The results are shown in Fig. 9:

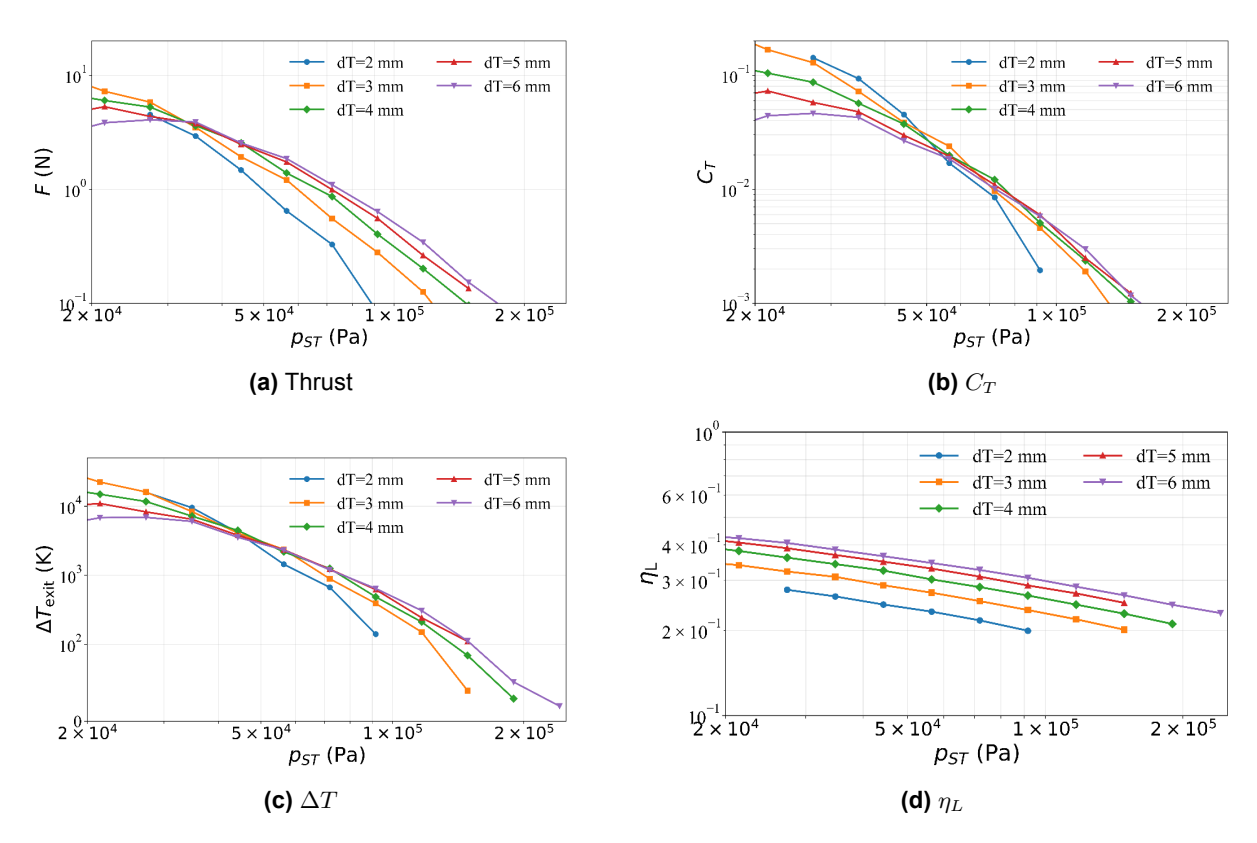


Fig 9. EP engine performance metrics for E=7.5 kV/m, for M7B nozzle conditions

A key observation is that the lorentz efficiency for these conditions is relatively poor, smaller than 40 % in most cases. This means that more energy is spent on rising the temperature of the flow rather than adding momentum to it. This is illustrated by the significant engine exit temperature rises in Fig. 9 (c), of up to 20,000 K. Accurately solving the MHD flow at these temperatures (above a few thousand K), considering the very simplifying assumptions that were made, is not realistic with the MHD solver used in this study. At such conditions the argon gas would be become fully electronically excited and ionized, and the actual bulk gas temperature would not reach such high values. A suitable kinetics model should

be implemented so that scenarios with high Joule heating can be better modeled.

Thrust values of nearly 10 N are nonetheless observed, for the flow conditions with the highest electrical conductivity values. The mechanism for thrust production in this context is better understood when taking a look at the spatially resolved acceleration profiles, shown in Fig. 10, and taking the example of the 5000 m/s conditions described in Table 1. It is apparent here that the flow velocity actually decreases along the engine channel, while pressure and temperature increase due to Joule heating. The thrust in this case comes from the higher pressure in the now underexpanded channel exit.

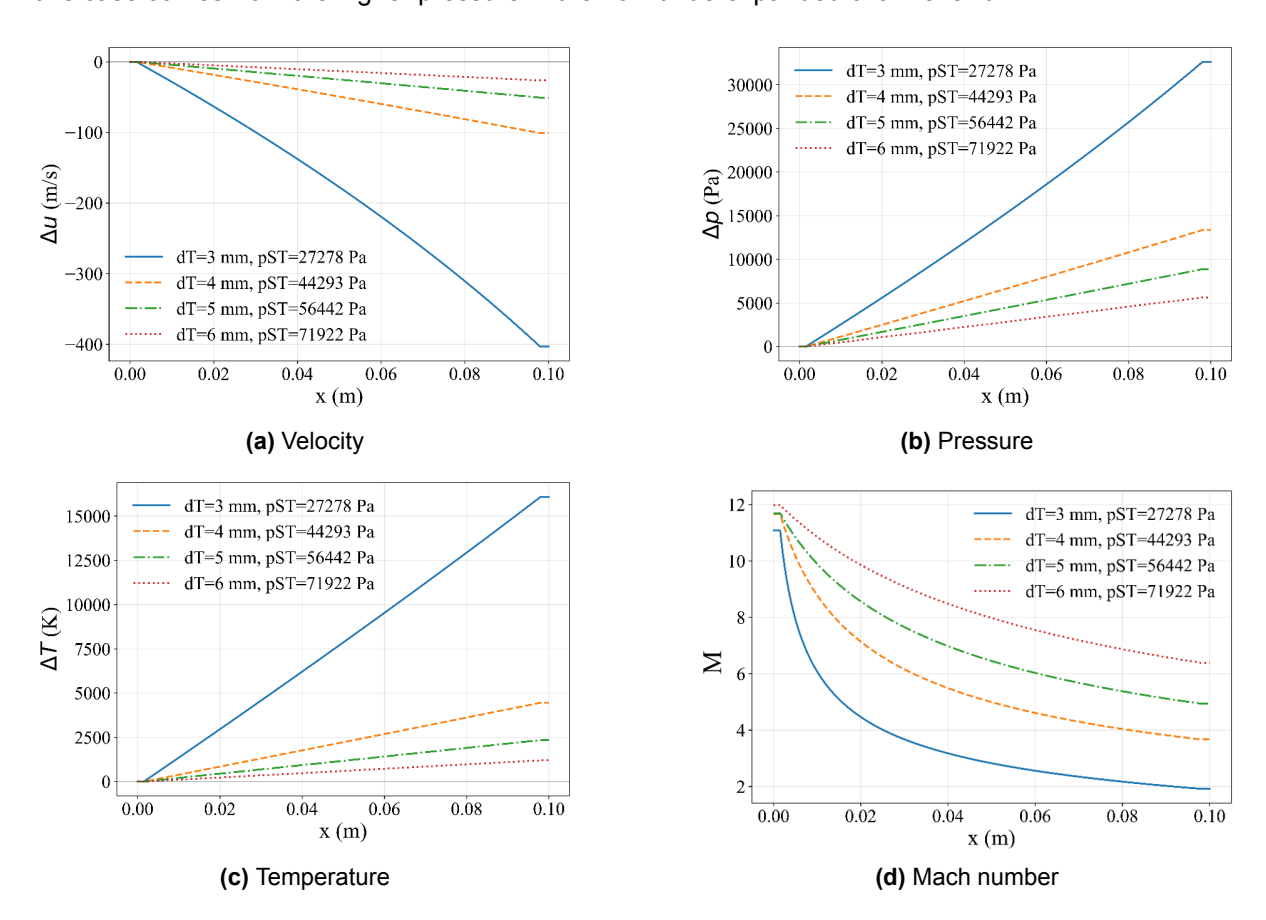


Fig 10. Quasi-1D solutions of spatial acceleration in the EP engine channel, for the conditions listed in Table 1, with E = 7.5 kV/m

These preliminary results suggest that an electromagnetic propulsion engine should aim to control Joule heating so that it is kept within reasonable levels, in particular so that no significant thermal ionization occurs, and also to maximize the Lorentz efficiency. While the overall efficiency of energy conversion into thrust can theoretically be restored by placing a diverging nozzle at the end of the MHD acceleration channel, or by having a variable area, diverging channel, this solution is limited by the available area ratio. Firstly, the electric field should be limited so that Joule heating is reduced during the MHD acceleration phase.

3.3.3. High efficiency acceleration

An acceleration loading factor can be defined, which describes how much initial Lorentz force (and Joule heating) is transferred to the test flow:

$$K = \frac{E_y}{u_x B_z} \tag{17}$$

Page I 13

The Lorentz efficiency is proportional to 1/K. The more loading is applied, the less fraction of the input power required to produce the E, B fields actually goes to increase the flow momentum. The induced current and Joule heating can be expressed as functions of K and σ :

$$j = \sigma u B(K - 1) \tag{18}$$

and

$$q_J = \sigma u B \times K(K-1) \tag{19}$$

For constant electric field acceleration, an upper limit of $K_{max}=1.2$ was found to yield acceptable temperature rises as a result of Joule heating. For the conditions listed in Table 1, this corresponds to an applied electric field of 3 kV/m, and the resulting acceleration profiles are shown in Fig. 11:

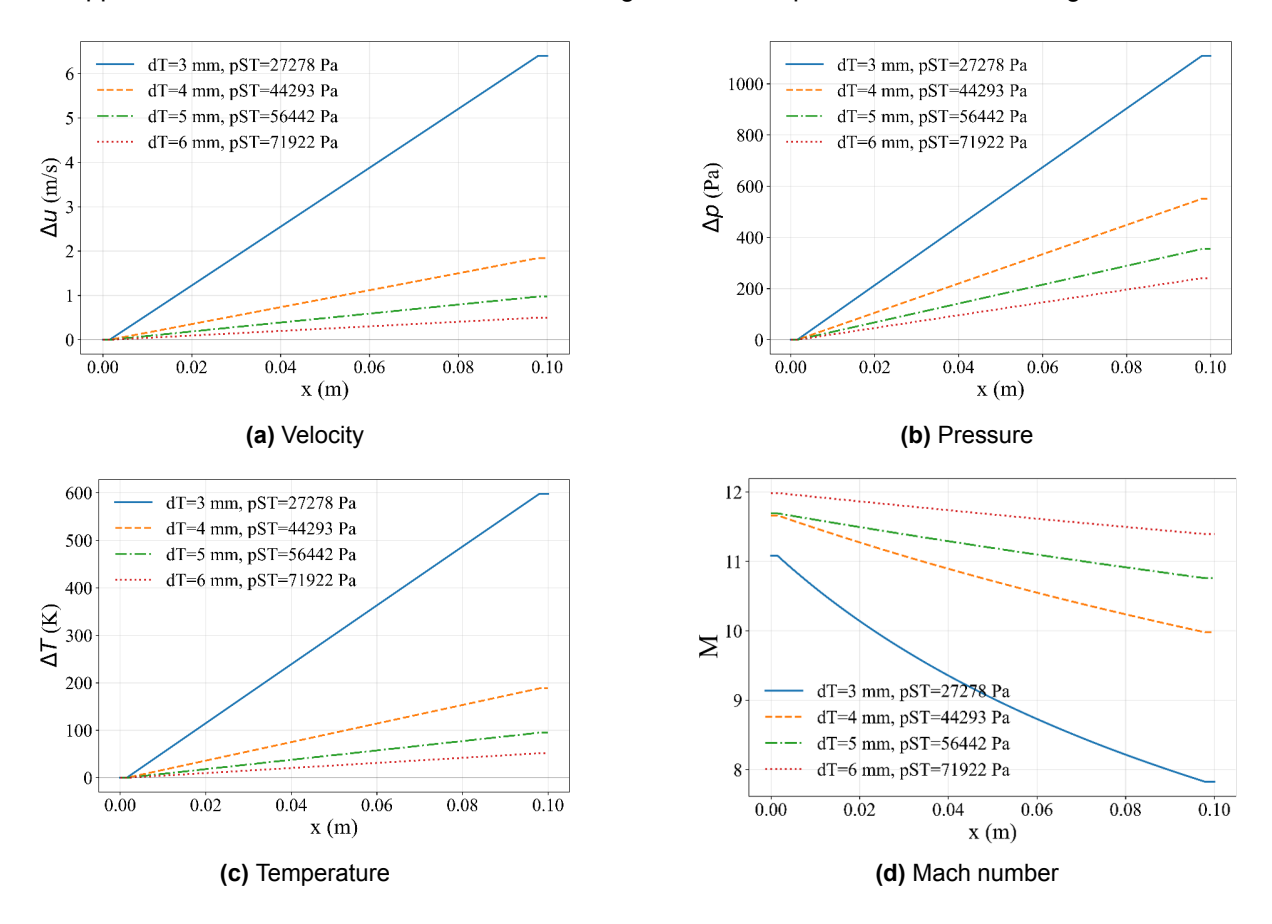


Fig 11. Quasi-1D solutions of spatial acceleration in the EP engine channel, for the conditions listed in Table 1, with E = 3 kV/m (K=1.2)

As seen in Fig. 11, the temperature rise due to Joule heating can be succesfully curbed by placing a limit on the loading parameter, with $\Delta T_{max}\approx 600K$ across the four conditions considered. A more complete approach would also take into account the electrical conductivity of each condition to limit the value of q_J per EQ. 19, which should also be normalized by the total flow enthalpy for example. The loading factor is nonetheless a simple and convenient parameter to use as reference, and is often used in the literature. Applying $K_{max}=1.2$ proved sufficient to provide a more realistic simulation space for the MHD solver in this study.

The maximum increase in velocity in this controlled heating environment is only around 6 m/s, which is not significant compared to the initial flow velocity.

3.3.4. Discussions

The results presented in this study suggest that this particular experimental configuration would not be sufficiently efficient to produce significant momentum changes. Nonetheless, the proposed concept could provide a very simple experimental implementation where significant Joule heating can be produced with only 100-200V of potential difference across the electrode pairs, and with affordable, off-theshelf permanent magnets. Joule heating is an important mechanism in MHD-controlled plasma and has drastic effects on the flow properties (pressure, temperature). In more severe cases, the corresponding energy source can couple with the flow chemistry and affect electrical conductivity, and potentially lead to instabilities when electromagnetic fields are applied [1]. An experimental investigation with suitable instrumentation, such as surface pressure and temperature sensors, could provide valuable data for the validation of CFD models that aim to simulate electromagnetic propulsion.

Future experiments should, however, aim to improve the Lorentz efficiency so that significant acceleration and thrust can be produced. Per EQ. 8, the term $\sigma(E-uB)B$ should be increased, without relying only on the electric field (which increases Joule heating). In the context of using permanent magnets, higher magnetic flux densities could be produced (up to 0.8T) by stacking a large number of magnets together. However, the value of 1T often used as reference in the literature is only accessible to electromagnets, which require a more complex experimental implementation.

The electrical conductivity was imposed by the set of flow conditions developed with the M4B and M7B nozzles. Other nozzles are available at T4 with higher area ratios (up to 1580 for the T4-M10 nozzle). It is possible that these could freeze the electron recombination reactions earlier in the expansion, thus leaving higher ionization fractions in the exit test flow. This would increase the electrical conductivity and improve the engine efficiency.

The application of a constant electric field along the entire engine channel is also inherently inefficient. A more optimized approach would be to dynamically increase E as the velocity increases, so that E-uBremains constant. Using this approach, a rate of acceleration can be maintained that is small enough to keep Joule heating small, and also large enough to produce significant acceleration of the flow.

4. Conclusion

The results presented in this study suggest that significant pre-ionization of argon test flows can be produced, which could be useful for future electromagnetic propulsion experiments. In future studies, experimental characterization of the argon test gas processes in T4 should be performed, which would allow empirical tuning of the L1D and NENZF1D simulation tools. More accurate predictions of the test flow conditions may then be made. The quasi-1D MHD code presented in this study was intended to be a computationally cheap and simple tool to evaluate the key plasma parameters and the MHD acceleration performance metrics. Once a few conditions of interest are selected, more complex CFD should be performed (using the in-house Eilmer5 code for example [13, 14, 15, 16]), to include boundary layer modeling, electrode sheaths, asymmetric Hall terms, finite-rate chemistry, and distribution of Joule heating and electron beam energy into the multiple energy modes of the test gas. For a rectangular channel, in particular, the problem is three-dimensional and should be solved as such. This effort is already in progress at UQ's Centre for Hypersonics, and draws on previous efforts of modeling nonequilibrium weakly ionized plasma relevant to electromagnetic propulsion, in particular by Parent et al. [17, 18] and Macheret et al. [1].

5. Acknowledgements

This research was supported by the Australian Government through the Australian Research Council's Linkage Projects scheme (project LP200200903), with Lockheed Martin and Lockheed Martin Australia as linkage partners.

References

- [1] Sergey O. Macheret, Mikhail N. Shneider, Richard B. Miles, and Ronald J. Lipinski. Electron-beam-generated plasmas in hypersonic magnetohydrodynamic channels. *AIAA Journal*, 39:1127–1138, January 2001.
- [2] Thomas Kava, John Evans, and Iain D. Boyd. Numerical simulation of electron-beam powered plasma fueled engines. In AIAA Propulsion and Energy 2021 Forum. American Institute of Aeronautics and Astronautics, July 2021.
- [3] R.J. Stalker, A. Paull, D.J Mee, R.G. Morgan, and P.A. Jacobs. Scramjets and shock tunnels—the queensland experience. *Progress in Aerospace Sciences*, 41(6):471–513, August 2005.
- [4] David J. Mee, R. G. Morgan, Allan Paull, P. A. Jacobs, and Michael K. Smart. *The T4 Stalker Tube*, page 1425–1429. Springer International Publishing, 2017.
- [5] Tony Arber. Fundamentals of magnetohydrodynamics (mhd). Lecture Handout, University of Warwick, UK, 2013.
- [6] Yuri P. Raizer. Gas Discharge Physics. Springer Berlin Heidelberg, 1991.
- [7] Peter A Jacobs. Shock tube modelling with I1d. 1998.
- [8] P. A. Jacobs. Quasi-one-dimensional modeling of a free-piston shock tunnel. *AIAA Journal*, 32(1):137–145, January 1994.
- [9] Peter Jacobs and Rowan Gollan. Implementation of a compressible-flow simulation code in the d programming language. *Applied Mechanics and Materials*, 846:54–60, July 2016.
- [10] Wilson Y. K. Chan, Peter A. Jacobs, Michael K. Smart, Samuel Grieve, Christopher S. Craddock, and Luke J. Doherty. Aerodynamic design of nozzles with uniform outflow for hypervelocity ground-test facilities. *Journal of Propulsion and Power*, 34(6):1467–1478, November 2018.
- [11] Martin I Hoffert and Hwachii Lien. Quasi-one-dimensional, nonequilibrium gas dynamics of partially ionized two-temperature argon. *The physics of Fluids*, 10(8):1769–1777, 1967.
- [12] Friedrich Paschen. Ueber die zum funkenübergang in luft, wasserstoff und kohlensäure bei verschiedenen drucken erforderliche potentialdifferenz. Annalen der Physik, 273(5):69–96, January 1889.
- [13] Nicholas N. Gibbons, Kyle A. Damm, Peter A. Jacobs, and Rowan J. Gollan. Eilmer: An open-source multi-physics hypersonic flow solver. *Computer Physics Communications*, 282:108551, jan 2023.
- [14] Peter Jacobs and Rowan Gollan. Implementation of a compressible-flow simulation code in the d programming language. *Applied Mechanics and Materials*, 846:54–60, jul 2016.
- [15] R.J. Gollan and P.A. Jacobs. About the formulation, verification and validation of the hypersonic flow solver eilmer. *International Journal for Numerical Methods in Fluids*, 73(1):19–57, mar 2013.
- [16] Kyle A. Damm, Rowan J. Gollan, Peter A. Jacobs, Michael K. Smart, Seonguk Lee, Eunsa Kim, and Chongam Kim. Discrete adjoint optimization of a hypersonic inlet. *AIAA Journal*, 58(6):2621–2634, June 2020.
- [17] Bernard Parent, Mikhail N. Shneider, and Sergey O. Macheret. Detailed modeling of plasmas for computational aerodynamics. *AIAA Journal*, 54(3):898–911, mar 2016.
- [18] B. Parent, P. Thoguluva Rajendran, and A. Omprakas. Electron losses in hypersonic flows. *Physics of Fluids*, 34(1), January 2022.